Solid State Phenomena
ISSN: 1662-9779, Vol. 388, pp 171-178
doi:10.4028/p-Hp3vb8

Submitted: 2026-01-19
Revised: 2026-02-16
Accepted: 2026-02-16
Online: 2026-04-15

Formability Test for Characterizing the Mode II–III Fracture Transition

Inês M. Almeida[1,a*], João P. G. Magrinho[1,b] Paulo A. F. Martins[1,c] and M. Beatriz Silva[1,d]

[1]IDMEC, Instituto Superior Técnico, Universidade de Lisboa, Av. Rovisco Pais, 1049-001 Lisboa, Portugal

[a*]ines.matias.almeida@tecnico.ulisboa.pt, [b]joao.magrinho@tecnico.ulisboa.pt, [c]pmartins@tecnico.ulisboa.pt, [d]beatriz.silva@tecnico.ulisboa.pt

[*]corresponding author

Keywords: sheet-bulk forming, fracture forming limits, sheet compression test.

Abstract. The transition between different shear fracture modes is still not well understood, especially in the case of mode II to mode III fracture. While transitions involving mode I have been investigated in previous studies, the interaction between in-plane and out-of-plane shear fracture remains largely unexplored. This work presents an ongoing study aimed at analysing this transition through a newly proposed formability test based on the compression of a thick sheet. The test is intended to investigate the transition region between the shear fracture forming limit (SFFL) and the out-of-plane shear fracture forming limit (OSFFL), associated with fracture mechanics modes II and III, respectively. A new specimen geometry was developed by combining features of existing configurations designed to activate each fracture mode separately. Finite element simulations were carried out to support the design of the specimen and to provide an initial analysis of the strain loading paths in the ligament region. Preliminary numerical results indicate that the proposed test can promote in-plane shear, out-of-plane shear, as well as mixed fracture mechanisms. The predicted fracture initiation sites and corresponding strain paths were examined in the effective strain–stress triaxiality space to provide initial insight into the role of stress state on fracture behaviour. The influence of notch orientation on the resulting fracture mode is discussed, highlighting the potential of the proposed approach for studying mixed shear fracture conditions.

Introduction

Accurate definition of deformation limits is essential for the optimization of metal forming processes and the prevention of fracture in metallic components [1]. Formability describes the ability of a material to sustain plastic deformation without failure and is commonly limited by necking or fracture. In sheet metal forming, fracture can occur through different crack-opening mechanisms, namely Mode I (tensile), Mode II (in-plane shear), and Mode III (out-of-plane shear) [2].

Formability is often represented using Forming Limit Diagrams (FLDs), where different fracture forming limits are associated with distinct fracture modes: the Fracture Forming Limit (FFL) for Mode I, the Shear Fracture Forming Limit (SFFL) for Mode II, and the Out-of-Plane Shear Fracture Forming Limit (OSFFL) for Mode III. While FLDs are widely used, their assumption of plane stress conditions limits their applicability, particularly when out-of-plane shear fracture is involved. To overcome this limitation, fracture behaviour can be represented in terms of effective strain and stress triaxiality, providing a more general framework to describe different fracture modes which was originally proposed by Vujovic and Shabaik [3].

Various experimental tests have been proposed to characterize each fracture forming limit individually. Tensile and bulge-based tests are commonly used to determine the FFL, a limit initially proposed by Atkins [4], while notched tensile and shear-based tests are employed to characterize the SFFL, a limit initially observed by Embury and Duncan [5] and later investigated by Marciniak [6]. Similarly, compression-based tests have been developed to activate Mode III fracture and determine the OSFFL [10]. Although transition regions between Mode I–Mode II and Mode I–Mode III fracture

have been investigated using dedicated specimen geometries, the transition between Mode II and Mode III fracture remains largely unexplored [7, 8].
Currently, no formability test exists that allows the systematic characterization of the transition between in-plane and out-of-plane shear fracture while accounting for both plane stress and three-dimensional material flow conditions. The objective of this work is therefore to propose a new formability test capable of investigating the transition zone between the SFFL and the OSFFL, providing initial insight into mixed shear fracture conditions.

Specimen Design

Based on the goal defined in the previous section, two main requirements were defined to guide the development of the proposed formability test for thick sheet materials. First, the specimen should be capable of failing under a combined in-plane and out-of-plane shear loading condition, corresponding to a mixed Mode II–Mode III fracture mechanism. Second, the experimental setup should prioritize simplicity to facilitate specimen fabrication, streamline testing conditions, and enable future modifications to the configuration.
Considering these requirements, a subset of five existing test configurations was selected for further evaluation. These tests are summarized in Table 1, and the rolling direction of the metal sheet is aligned in the arrows in the first three and fifth and regarding the double notched compression test, is perpendicular to the loading direction.

Table 1. Five selected tests based on the key characteristics of each. The information regarding the Double-Notched Shear Test is derived from [9], while the data for the other tests is based on the work of [10].

Double Notched Tensile	Staggered Double Notched Tensile	Shear	Double notched Compression	Sheet Lenghtwise Compression
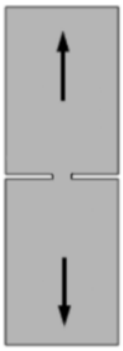	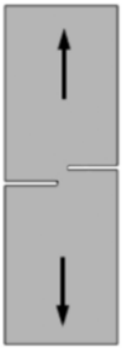		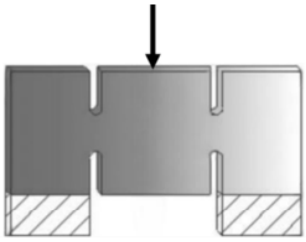	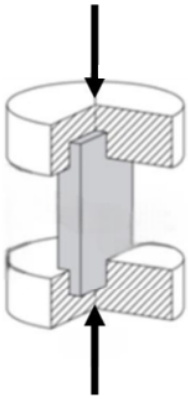
Mode I	Mode I and II	Mode II	Mode II	Mode III

The first three tests in Table 1, the double-notched tensile, staggered double-notched tensile, and shear tests, primarily involve tensile loading. This limits their ability to explore fracture modes beyond Mode I and Mode II. Despite this, the notch geometry in these tests is an important factor, as the angle and shape of the notches influence the development of mixed-mode fracture.
Previous research has shown that compressive forces can significantly affect fracture behaviour in thick sheets. Silva et al. [9] found that applying compression near the notches in a double-notched shear test can induce Mode II fracture, which is useful for evaluating fracture toughness. Similarly, Leonardo et al. [10] demonstrated that compressing a sheet along its length on both sides induces Mode III fracture, with cracks initiating and propagating through the sheet thickness.
Drawing inspiration from these tests, a new specimen design was developed by combining two critical features: the double-notch geometry and the application of compressive loads. The goal of the new design is to create a stress concentration in the notched region that drives material movement through

the thickness, producing out-of-plane stresses. A schematic of the proposed geometry, along with the main dimensions, is shown in Figure 1.

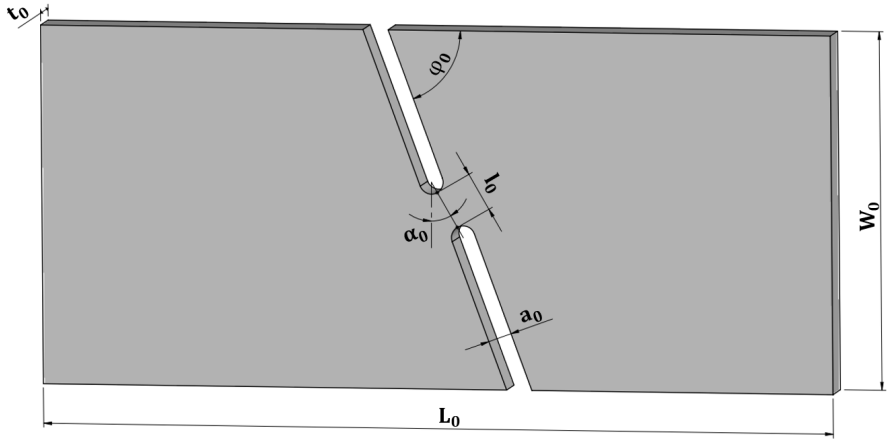

Fig. 1. Schematic representation of the specimen with geometrical parameters identified: angle between notches (α_0), ligament size (l_0), notch width (a_0), notch angle (φ_0), width (W_0), length (L_0) and thickness (t_0).

The geometric parameters of the specimen are defined as follows. The notch-to-notch angle, α_0, is measured between the vertical axis and the line connecting the centres of the two notch arcs. The ligament length, l_0, corresponds to the minimum distance separating the notches, while the notch width, a_0, represents the horizontal extent of each notch. The notch inclination, φ_0, is defined as the angle between the notch edge and the horizontal axis. In addition, the overall specimen dimensions are described by its width W_0, length L_0, and thickness t_0.
Each parameter was analysed individually, while the others were maintained at their reference values. The parameter values tested and their corresponding reference values are shown in Table 2. It is important to note that the thickness parameter will not be evaluated, as the sheet used in the tests had a thickness of 5 mm.

Table 2. Geometric parameter values tested and their corresponding reference values.

Parameters	Values Tested							Reference Value
Angle between notches α_0 [º]	0	15	30	45	60	75	90	45
Ligament Sizes l_0 [mm]	2.5	5	7.5	10	12.5	15		5
Notch Width a_0 [mm]	2	3	4	5	6			3
Notch Angle φ_0 [º]	30	45	60	75	90			70
Width W_0 [mm]	20	45	80					45
Length L_0 [mm]	50	100	150					100

Numerical Simulation

The parameters presented in Table 2 were evaluated using an in-house software, i-form 3D [2]. This software is based on a modified weak form of Markov's rate of energy variational statement, which accounts for contact and frictional sliding between the specimens and the various tool components of the experimental setup and it is used to solve quasi-static problems.

$$\int_V \sigma'_{ij}\delta D_{ij}dV + \int_V \sigma_m \delta D_v dV - \int_{S_t} t_i\,\delta u_i dS + \int_{S_f}\left(\int_0^{|u_r|}\tau_f \delta u_r\right)dS = 0 \quad (1)$$

The weak form above adopts a control volume V approach incorporating a sort of 'updated Eulerian approach' with velocities u_i as the primary unknowns [11]. The first term of the expression involves the deviatoric Cauchy stress σ'_{ij} and the rate of deformation D_{ij}, representing viscous effects. The second term makes use of the hydrostatic stress σ_m and the volumetric rate of deformation D_v, analogous to hydrostatic effects on a viscous fluid. The incompressibility condition of the velocity field $D_v = 0$ is relaxed using a penalty function K, where $\sigma_m = (K/2)D_v$.
The third and fourth terms in (1) refer to the tractions t_i applied on the boundary S_t of the control volume, and to the friction shear stress τ_f and the relative sliding velocity u_r acting on the contact interfaces S_f between the specimens and the various tool components. Friction was modelled using the law of constant friction, expressed as $\tau_f = mk$, where k represents the shear flow stress and m denotes the friction factor which was taken as 0.05.
The Hill criterion [12] was used to better capture the material's anisotropic behaviour, since anisotropic effects became more critical due to the consideration of stresses in all directions. The anisotropy parameters (F, G, H, L, M, N), which define the shape of the yield surface in the stress space, indicating how much the material deviates from isotropic behaviour, were previously calculated by [10] as well as the remain material properties and are presented in Table 3. These were input into the software to accurately represent the sheet's material properties. The material properties determined and presented in table 3 are the Young Modulus E, the yield stress σ_Y, the ultimate tensile stress σ_{UTS}, the elongation at break A, and planar anisotropy $\bar{r}$.

Table 3. Mechanical properties and anisotropy parameters of the aluminium AW7075-T651 sheets obtained from tensile tests by Leonardo (2019).

Properties	E (GPa)	σ_Y (MPa)	σ_{UTS} (MPa)	A [%]	$\bar{r}$	Anisotropy parameters					
						F	G	H	L	M	N
Values	71.72	520.52	584.67	14.55	0.663	0.4493	0.6523	0.3477	3.0000	3.0000	1.2907

The model used in the numerical simulations is shown in Figure 2. The specimen is a deformable object modelled with around 60 000 solid hexahedral quadratic elements varying slightly depending on the ligament size, with mesh refinement in the ligament to improve simulation results in this region, which experiences higher deformation. The tool was modelled with contact-friction spatial triangles.

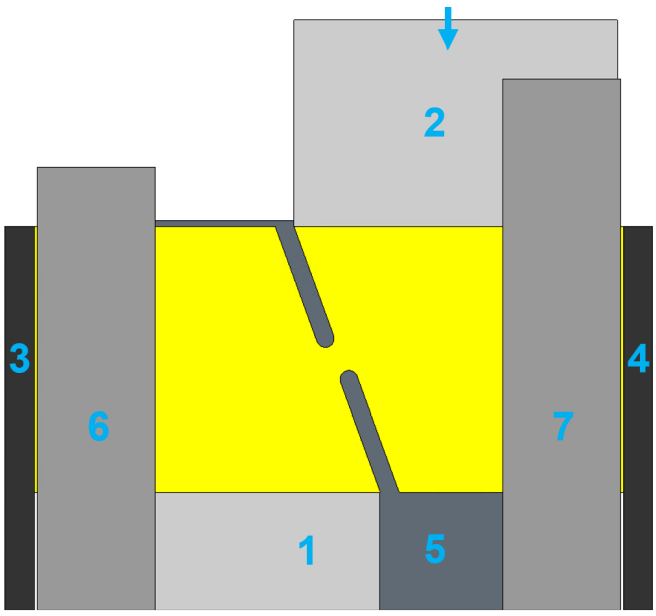

Fig. 2. Schematic representation of the model and finite element mesh used to simulate the new proposed test showing: (1) the lower support, (2) the punch, (3) and (4) the lateral supports, (5) the back support, and (6-7) the front supports.

In this model, the lower support (1) serves as the base for positioning and securely fixing the specimen. The punch (2) applies a downward force, while the lateral (3 and 4), front (6 and 7), and back (5) supports maintain near-pure shear conditions. All tools are modelled as rigid bodies, with all components remaining stationary during the simulation except for the punch (2), which moves downward at a constant speed.
All simulations were performed, and results were extracted at the centre of the ligament area between the two notches, where the highest shear stresses are anticipated.

Results and Discussion

The numerical results used to plot the loading evolutions in the effective strain versus stress triaxiality space $\bar{\varepsilon} = f(\eta)$ were extracted from the central point of the ligament area between the two notches, as this region is anticipated to experience the highest shear stresses. The effective strain versus stress triaxiality space $\bar{\varepsilon} = f(\eta)$ was selected over the principal strain space $\varepsilon_1 = f(\varepsilon_2)$ because the latter does not adequately account for regions opposite surface of the specimens in contact with the back support (5), exhibiting local deviations from plane stress conditions.

Geometric Sensibility Analysis.

The simulations were terminated when the punch displacement reached 3 mm for all specimens. Although this displacement may not coincide with the exact moment of fracture, this approach was used because the objective was to analyse deformation up to, but not necessarily at, the fracture point.

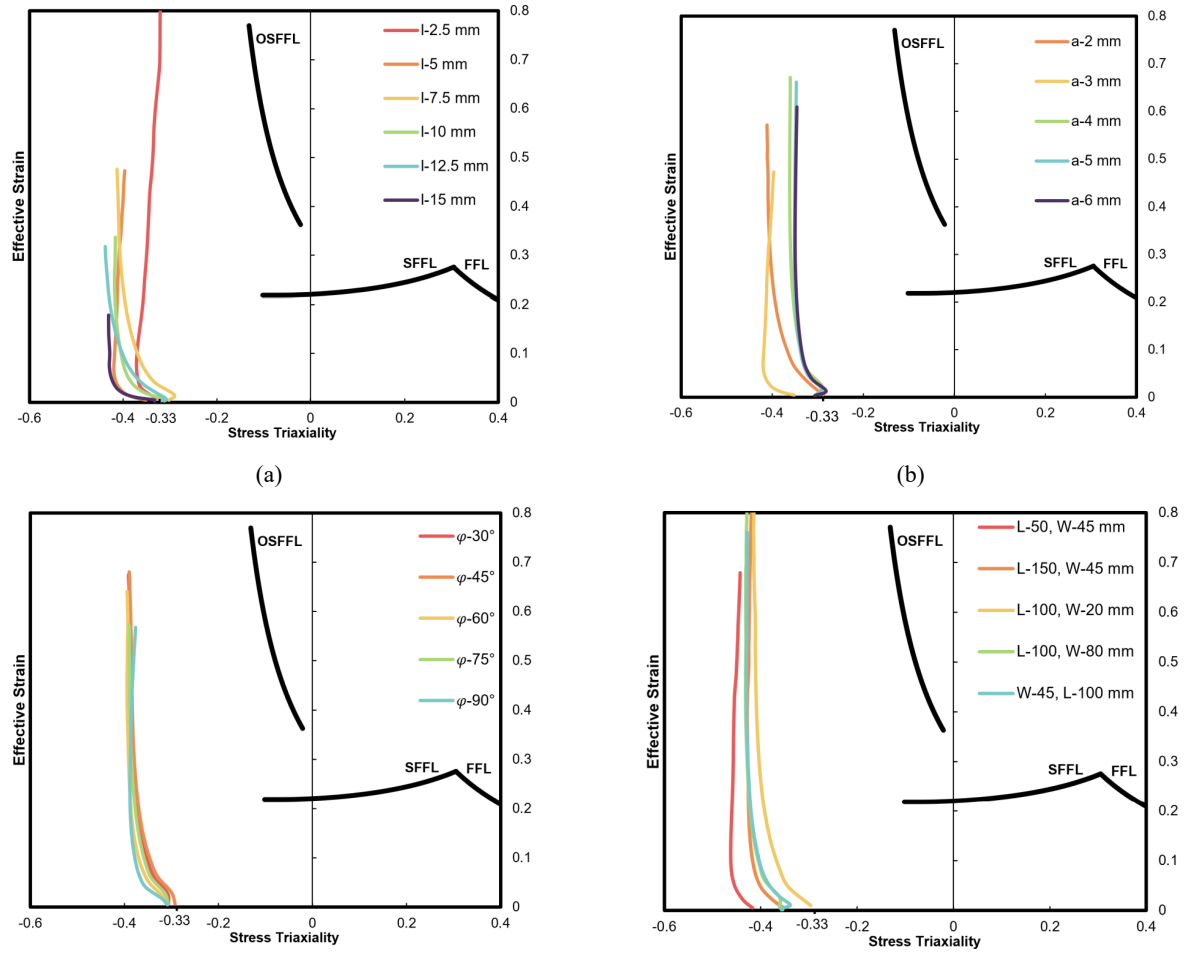

Fig. 3. Loading paths in the effective strain vs. stress triaxiality space $\bar{\varepsilon} = f(\eta)$ for various specimen parameters: (a) ligament size (l_0), (b) notch width (a_0), (c) notch angle (φ_0), and (d) combined width (W_0) and length (L_0).

Figure 3a presents the ligament size analysis (l_0), demonstrating that triaxiality values are consistent across all sizes, remaining below $\eta = -1/3$ (indicative of uniaxial compression) but above $\eta = -2/3$ (associated with equi-biaxial compression). The results further show that increasing ligament size leads to higher compressive stresses within the notch area and lower maximum effective strain values, indicating reduced strain accumulation in specimens with larger ligament sizes.
Figure 3b shows that, in the analysis of notch width (a_0), the evolution of triaxiality remains nearly constant for widths greater than 3 mm, with values around $\eta = -1/3$, which indicates uniaxial compression. For these widths, compressive stress is primarily oriented in a single direction. In contrast, widths of 2 mm and 3 mm produce higher stress concentrations due to the smaller notch, resulting in compressive stresses in multiple directions and triaxiality values $\eta < -1/3$.
Figure 3c demonstrates that triaxiality values $\eta \approx -0.4$ remain approximately constant across different notch angles (φ_0), indicating that this parameter exerts minimal influence on the results. The changes in triaxiality previously observed are, therefore, attributed to the influence of other parameters, which were now kept at their reference values. Similarly, Figure 3d shows no dependence of the results on the specimen's length (L_0) or width (W_0).
Based on these results, a detailed analysis was conducted for all notch-to-notch angles α_0 in specimens with a notch size $l_0 = 5$ mm, since it is a common practice to choose a value that matches the sheet thickness and none of the other tested values produced significant deviations. A notch width $a_0 = 3$ mm was employed in agreement with previous studies performed on staggered double-notched tension [10] and double-notched shear tests [9]. Since the notch angle φ_0 did not influence the results, a reference value of $\varphi_0 = 70^{\circ}$ was selected for all specimens.
The remaining specimen dimensions were set at $L_0 = 100$ mm and $W_0 = 45$, following a previous work of Silva et al. [9].

Strain Evolution.

Firstly, the effective strain for all the specimens were analysed to understand if the deformation was in fact, localized in the ligament, which was verified. An example of this localization can be seen in figure 4 for the specimen with a ligament angle of 0º.

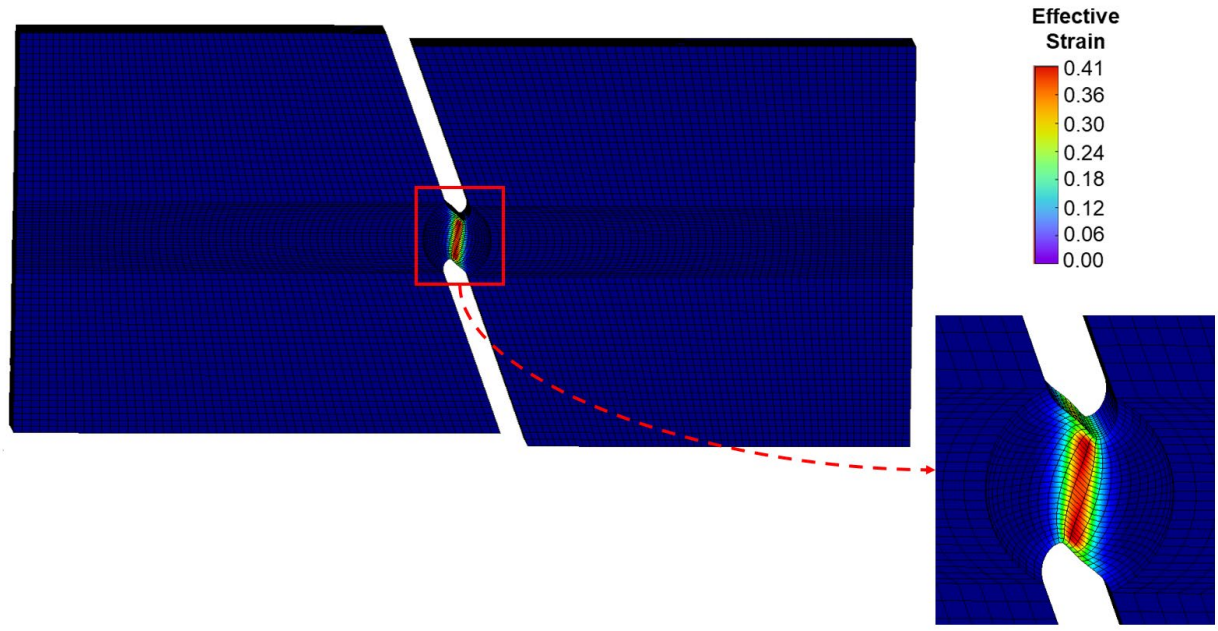

Fig. 4. Effective Strain distribution in the last step of the numerical simulation of the specimen with $\alpha_0 = 0°$.

To characterize the shear stresses experienced by the different specimens and how they influence the overall strain distribution, the strain loading paths were represented in the effective strain vs. triaxiality plane in combination with the FFL, SFFL, and OSFFL previously determined by Leonardo

et al. [10] (see Figure 5). The strain loading paths were obtained from the numerical simulations after a punch displacement of 3 mm, assuming that the specimen exhibits no lateral movement and full contact with the tools, which helps explaining why the loading paths extend beyond the limits previously determined by conventional tests.

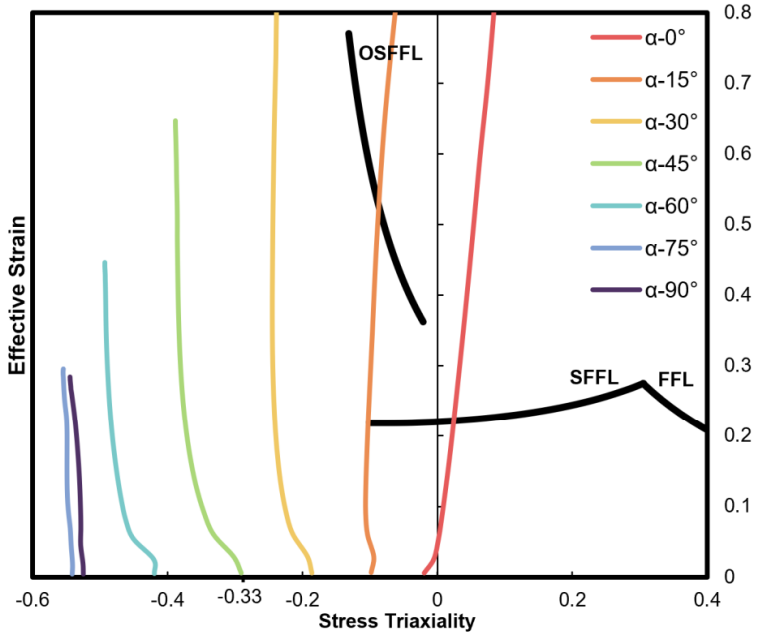

Fig. 5. Graphical representation in the triaxiality space of FFL, SFFL and OSFFL, along with the numerical triaxiality paths of the specimens with different angle between notches.

An overall increase in stress triaxiality is observed as the notch-to-notch angle α_0 increases. For specimens with notch-to-notch angles α_0 equal to 0° and 15°, the loading trajectories intersect the SFFL and extend beyond it prior to fracture. This behaviour is likely a result of fixing the amount of punch displacement independently of the specimen geometry and likely also a result of compressive loading conditions imposed by specimen constraints, which intensify stress localization within the ligament and result in higher effective strain levels as the loading paths approach pure shear ($\eta = 0$). In contrast, specimens with α_0 of 30° and 45°, display loading paths that begin at relatively low triaxiality values and progressively approach the SFFL as deformation advances. In these cases, fracture occurs in a region between the SFFL and OSFFL, indicating the activation of a mixed in-plane and out-of-plane shear fracture mechanism.

For specimens with notch-to-notch angles $\alpha_0 > 60°$, the deformation path begins at negative triaxiality values ($\eta < -0.40$), which increase as the angle increases. This trend demonstrates the presence of significant compressive stresses and indicates that fracture is dominated by out-of-plane shear, corresponding to Mode III.

Overall, the proposed specimen configuration seems capable of generating strain loading paths representative of fracture under Mode II, Mode III, and mixed Mode II–III conditions for notch-to-notch angles α_0 ranging from 0° and 60°. Therefore, specimens with larger notch angles (e.g., $\alpha_0 =$ 75° and 90°) are unnecessary to achieve the required objectives.

Conclusion

A novel formability test was proposed and validated numerically, utilizing the compression of thick sheets to characterize the transition zone between the shear fracture forming limit (SFFL, Mode II) and the out-of-plane shear fracture forming limit (OSFFL, Mode III).

Finite element modelling was employed to optimize specimen geometry and demonstrated that the test promotes both in-plane and out-of-plane shear mechanisms as the angle between the notches α_0 is varied.

References

[1] P.A.F. Martins, N. Bay, A.E. Tekkaya, A.G. Atkins, Characterization of fracture loci in metal forming, Int. J. Mech. Sci. 83 (2014) 112–123.

[2] C. Nielsen, P. Martins, *Metal Forming: Formability, Simulation, and Tool Design*, Elsevier Science, 2021.

[3] V. Vujovic, A.H. Shabaik, A new workability criterion for ductile metals, J. Eng. Mater. Technol. 108 (1986) 245–249.

[4] A.G. Atkins, Fracture in forming, J. Mater. Process. Technol. 56 (1996) 609–618.

[5] J. Embury, J. Duncan, Formability maps, Annu. Rev. Mater. Sci. 11 (1981) 505–521.

[6] Z. Marciniak, Assessment of material formability, Adv. Technol. Plast. 1 (1984) 685–694.

[7] J.P. Magrinho, M.B. Silva, L. Reis, P.A.F. Martins, Formability limits, fractography and fracture toughness in sheet metal forming, Materials 12 (2019) 1493.

[8] J.P. Magrinho, M.B. Silva, L.M. Alves, A.G. Atkins, P.A.F. Martins, New methodology for the characterization of failure by fracture in bulk forming, J. Strain Anal. Eng. Des. 53 (2018) 242–247.

[9] C. Silva, M. Silva, L. Alves, P.A.F. Martins, A new test for determining the mechanical and fracture behavior of materials in sheet-bulk metal forming, Proc. Inst. Mech. Eng. Part L: J. Mater. Des. Appl. 231 (2017) 1–12.

[10] P.N.C. Leonardo, J.P. Magrinho, I.M.F. Bragança, M.B. Silva, C.M.A. Silva, P.A.F. Martins, Formability limits in sheet-bulk forming, Int. J. Mach. Tools Manuf. 149 (2020) 103509.

[11] K. Mattiasson, FE-models of the sheet metal forming processes, in: D. Banabic (Ed.), *Sheet Metal Forming Processes: Constitutive Modelling and Numerical Simulation*, Springer-Verlag, 2010, pp. 1–24.

[12] R. Hill, A theory of the yielding and plastic flow of anisotropic metals, Proc. R. Soc. Lond. A 193 (1948) 281–297.